INTERNATIONAL JOURNAL FOR NUMERICAL AND ANALYTICAL METHODS IN GEOMECHANICS
Int. J. Numer. Anal. Meth. Geomech., **22**, 575–595 (1998)

CONTAMINANT TRANSPORT UNDER VARIABLE DENSITY FLOW IN FRACTURED POROUS MEDIA

S. VALLIAPPAN*, W. WANG AND N. KHALILI

School of Civil Engineering, University of New South Wales, Sydney 2052, Australia

SUMMARY

A numerical model for simulating flow and transport of contaminants with variable density in fractured porous media is presented. The non-linearities arising from the density variation and the velocty-dependent dispersion terms have been handled by Picard method. It is shown that the contaminant transport in a fractured porous medium is initially dominated by fractures. However, with time increasing, the contaminant concentration in porous blocks increases, due to the leakage of contaminant from the fracture network to the porous blocks. It is also shown that the high density of contaminant has a greater effect on its transport in the fracture network than in the porous blocks. © 1998 John Wiley & Sons, Ltd.

Key words: contaminant transport; variable density flow; fractures; leakage; dispersion; diffusion

1. INTRODUCTION

Due to increased environmental concerns, the flow and transport of contaminant in fractured porous media have received a great deal of attention in the past two decades. During this period, various mathematical models have been proposed for the solution of flow and transport problems. The most common assumption in these models is that the fluid flow is independent of the density of contaminant. While this assumption is valid for many contaminant plumes of low concentration, it is not valid for highly concentrated leachates where the density of fluid is not constant. In fact, the density of groundwater flow may vary considerably as a result of the presence of trace quantities of dissolved contaminants.[1, 2] Therefore, the effect of density on fluid flow should be considered. One of the most common practical situations where density driven flow is encountered is salt water intrusion in coastal aquifers.[3, 4] Other important applications include migration of dense organic contaminants and isolation of waste repositories in stable salt or in fractured rock formations.[5, 6]

Besides the works mentioned in the previous paragraph, further studies on fluid flow with variable density in porous media have been carried out by Schincariol *et al.*,[7] Zhang and Schwartz[8] and Wicks and Herman.[9] However, very few attempts have been made to study the variable density flow in fractured porous media. In a highly fractured porous medium, the transport behaviour of contaminants can be significantly altered by the presence of

* Correspondence to: S. Valliappan, School of Civil Engineering, University of New South Wales, Sydney 2052, Australia.

CCC 0363–9061/98/070575–21$17.50

Received 20 November 1996
Revised 26 September 1997

fractures.[10–14] Classical models that describes flow in fractured porous media are proposed by Barenblatt *et al.*[10] and Warren and Root[11] based on the double-porosity conceptual aproach. Later, Huyakorn *et al.*[12, 13] presented flow and contaminant transport models using the double-porosity concept. The exchange term was obtained by considering different types of matrix blocks. Employing the double-porosity concept, a semi-anlytical solution for simulating contaminant transport through fractured media was given by Rowe and Booker.[14] In the above models, the effects of variable density were not considered. Recently, Shikaze and Sudicky[15] studied the density-driven movement of organic vapours in fractured porous media. However, their work was primarily focused on flow through discretly fractured media in which the porous matrix was represented by rectangular elements and the fractures by one-dimensional line elements superimposed on the rectangular grid.

In this paper, a two-dimensional finite element model for the fully coupled analysis of variable density flow and transport of contaminant in naturally fractured porous media is presented. The effects of fluid density on concentration of contaminants in the fractured network and the porous blocks are considered separately. After a brief description of the governing equations, the finite element formulation of the model is presented.

The validity and the application of the model are demonstrated through a number of simple problems. The sensitivity of the results pertaining to the parameters selected is also investigated. The results show that the contaminant transport in fractured porous media is initially dominated by fractures. However, with increasing time, the contaminant concentration in the porous blocks increases, as the leakage from the fracture network to the porous blocks takes place. Eventually, at a later period, the concentration in the fracture network and the porous blocks approaches a similar value, but not corresponding to the equivalent homogeneous behaviour of the total system because of velocity-dependent dispersion.

The effect of fracture spacing on the contaminant transport in fractured porous media has also been investigated. Comparing the results for different spacings, it is shown that as the fracture spacing increases, the concentration in the fracture network increases whereas the concentration in the porous blocks decreases, as expected. This is due to a decrease in the leakage and the mass transfer between the fracture network and the porous blocks, which are inversely proportional to the fracture spacing.

2. THEORETICAL DEVELOPMENT

In this paper, a numerical model for the flow and transport of contaminant through fractured porous media based on the concept of double porosity is presented. In this concept, a fractured porous medium is idealized as two interacting continua: one representing the fracture mnetwork and the other representing the porous blocks. These two continua are in turn coupled through a leakage term,[16, 17] controlling the transfer of fluiid and contaminant between the fracture network and the porous blocks. The rate of fluid transfer at each point depends upon the fluid potential difference between the fracture network and the porous blocks, as well as the permeability and the geometry of the porous blocks. Similarly, the rate of mass transfer at each point depends on the concentration difference between the fracture network and the porous blocks, the diffusion coefficient, and the geometry of the porous blocks as well as the rate of fluid transfer between the two systems. The effects due to the density of contaminant in the fracture network and the porous blocks are considered separately. The flow and transport equations are coupled through the velocity terms and the concentration of contaminant.

Within this framework, the differential equations for flow in a fractured porous medium may be expressed as

$$\frac{\partial}{\partial x_i}\left[\rho_{\mathrm{m}}\frac{k_{\mathrm{m}ij}}{\mu_{\mathrm{m}}}\frac{\partial \Psi_{\mathrm{m}}}{\partial x_j}\right] = \rho_{\mathrm{m}} s_{\mathrm{m}}\frac{\partial p_{\mathrm{m}}}{\partial t} + \phi_{\mathrm{m}}\frac{\partial \rho_{\mathrm{m}}}{\partial c_{\mathrm{m}}}\frac{\partial c_{\mathrm{m}}}{\partial t} + \rho_{\mathrm{m}}\Gamma_1, \quad i,j = 1,2 \tag{1}$$

$$\frac{\partial}{\partial x_i}\left[\rho_{\mathrm{f}}\frac{k_{\mathrm{f}ij}}{\mu_{\mathrm{f}}}\frac{\partial \Psi_{\mathrm{f}}}{\partial x_j}\right] = \rho_{\mathrm{f}} s_{\mathrm{f}}\frac{\partial p_{\mathrm{f}}}{\partial t} + \phi_{\mathrm{f}}\frac{\partial \rho_{\mathrm{f}}}{\partial c_{\mathrm{f}}}\frac{\partial c_{\mathrm{f}}}{\partial t} - \rho_{\mathrm{f}}\Gamma_1, \quad i,j = 1,2 \tag{2}$$

$$\Gamma_1 = \eta(\Psi_{\mathrm{m}} - \Psi_{\mathrm{f}}) \tag{3}$$

where Ψ_{m} and Ψ_{f} are the fluid potential in the porous blocks and the fracture network, respectively, and are defined as $\Psi_{\mathrm{m}} = p_{\mathrm{m}} + \rho_{\mathrm{m}} gz$ and $\Psi_{\mathrm{f}} = p_{\mathrm{f}} + \rho_{\mathrm{f}} gz$, ϕ_{m}, ρ_{m}, μ_{m}, $k_{\mathrm{m}ij}$, s_{m} and p_{m} represent the porosity, fluid density, viscosity, average intrinsic permeability, specific storativity and fluid pressure in the porous blocks; ϕ_{f}, ρ_{f}, μ_{f}, $k_{\mathrm{f}ij}$, s_{f} and p_{f} represent the porosity, fluid density, viscosity, average intrinsic permeability, specific storativity and fluid pressure, respectively, in the fracture network; g is the gravity acceleration; ρ_{w} is the fresh water density; and z is the elevation above a reference datum.

Γ_1 is a leakage term, describing the rate of fluid flow from the porous blocks to the fracture network and *vice versa*, and η is the leakage parameter which is defined as a function of the porous blocks, permeability and average fracture spacing. Barenblatt *et al.*[10] and Warren and Root[11] proposed the following relationship for η:

$$\eta = \bar{\alpha}\frac{k_{\mathrm{m}}}{\mu_{\mathrm{m}}} \quad (\text{assuming } k_{\mathrm{m}11} = k_{\mathrm{m}22} = k_{\mathrm{m}}) \tag{4}$$

which is obtained assuming that a quasi-steady flow condition exists between the porous blocks and the fracture network; The factor $\bar{\alpha}$ is defined as

$$\bar{\alpha} = \frac{4n(n+2)}{l^2} \tag{5a}$$

where $n = 1, 2$ is the number of normal sets of fractures; and l is defined as

$$l = \frac{2D_1D_2}{D_1 + D_2} \quad \text{for } n = 2 \tag{5b}$$

$$= D_1 \qquad \text{for } n = 1$$

where D_1 and D_2 are the average fracture spacing along two orthogonal directions.

Idealizing a naturally fractured medium as an orthogonal network of equally spaced fractures, $k_{\mathrm{f}ij}$ can be estimated as[11]

$$k_{\mathrm{f}ij} = \frac{b^3}{12l}\delta_{ij} \tag{6}$$

where b represents the aperture width.

Similarly, the relationship between the spacing and the porosity for fractures can be defined as

$$\phi_{\mathrm{f}} = b\left(\frac{1}{D_1} + \frac{1}{D_2}\right) \tag{7}$$

The initial and boundary conditions necessary for the solution of equations (1) and (2) are:

$$p_{\mathrm{m}} = p_{\mathrm{m}0} \quad \text{when } t = 0$$

$$p_{\mathrm{f}} = p_{\mathrm{f}0} \quad \text{when } t = 0$$

$$p_{\mathrm{m}} = \bar{p}_{\mathrm{m}} \quad \text{on } S_{\mathrm{mw}1}$$

$$-\left[\frac{\mathrm{k}_{\mathrm{m}ij}}{\mu_{\mathrm{m}}}\left(\frac{\partial p_{\mathrm{m}}}{\partial x_j} + \rho_{\mathrm{m}} g \frac{\partial z}{\partial x_j}\right)\right] n_i = \bar{q}_{\mathrm{m}n} \quad \text{on } S_{\mathrm{mw}2}$$

$$p_{\mathrm{f}} = \bar{p}_{\mathrm{f}} \quad \text{on } S_{\mathrm{fw}1}$$

$$-\left[\frac{\mathrm{k}_{\mathrm{f}ij}}{\mu_{\mathrm{f}}}\left(\frac{\partial p_{\mathrm{f}}}{\partial x_j} + \rho_{\mathrm{f}} g \frac{\partial z}{\partial x_j}\right)\right] n_i = \bar{q}_{\mathrm{f}n} \quad \text{on } S_{\mathrm{fw}2}$$

where $p_{\mathrm{m}0}$ and $p_{\mathrm{f}0}$ are initial fluid pressure in the porous blocks and the fracture network; $\bar{p}_{\mathrm{m}}$ and $\bar{p}_{\mathrm{f}}$ represent the prescribed pressure on boundaries $S_{\mathrm{mw}1}$ and $S_{\mathrm{fw}1}$; $\bar{q}_{\mathrm{m}n}$ and $\bar{q}_{\mathrm{f}n}$ are the fluid fluxes normal to the boundaries $S_{\mathrm{mw}2}$ and $S_{\mathrm{fw}2}$, respectively.

The governing equations for the contaminant transport may be written as

$$\frac{\partial}{\partial x_i}\left[\phi_{\mathrm{m}} D_{\mathrm{m}ij} \frac{\partial c_{\mathrm{m}}}{\partial x_j}\right] - v_{\mathrm{m}i} \frac{\partial}{\partial x_i}(\phi_{\mathrm{m}} c_{\mathrm{m}}) = R_{\mathrm{m}} \phi_{\mathrm{m}} \frac{\partial c_{\mathrm{m}}}{\partial t} + \lambda R_{\mathrm{m}} \phi_{\mathrm{m}} c_{\mathrm{m}} + \Gamma_2, \quad i, j = 1, 2 \tag{8}$$

$$\frac{\partial}{\partial x_i}\left[\phi_{\mathrm{f}} D_{\mathrm{f}ij} \frac{\partial c_{\mathrm{f}}}{\partial x_j}\right] - v_{\mathrm{f}i} \frac{\partial}{\partial x_i}(\phi_{\mathrm{f}} c_{\mathrm{f}}) = R_{\mathrm{f}} \phi_{\mathrm{f}} \frac{\partial c_{\mathrm{f}}}{\partial t} + \lambda R_{\mathrm{f}} \phi_{\mathrm{f}} c_{\mathrm{f}} - \Gamma_2, \quad i, j = 1, 2 \tag{9}$$

$$\Gamma_2 = \beta(c_m - c_{\mathrm{f}}) + d_1 \frac{\Gamma_1}{\rho_{\mathrm{w}}} + (1 - d_1) \frac{\Gamma_1}{\rho_{\mathrm{w}}} c_{\mathrm{m}} \tag{10}$$

where Γ_2 is a term expressing mass exchange between the porous blocks and the fracture network; d_1 is a dimensionless coefficient which determines the direction of flow between the two systems, if $\Gamma_1 > 0$, $d_1 = 0$. and if $\Gamma_1 < 0$, $d_1 = 1$; the parameter β, which controls mass transfer between the porous blocks and the fracture network, can be obtained as

$$\beta = \bar{\alpha} \phi_{\mathrm{m}} D^*_{\mathrm{m}} \tag{11}$$

where D^*_{m} is the coefficient of molecular diffusion in the porous blocks; c_{m} and c_{f} are concentrations of contaminant in the porous blocks and the fracture network; λ is the first-order decay constant; R_{m} is retardation factor in the porous blocks and R_{f} is retardation factor in the fracture network.

The average linear velocities in the porous blocks and the fracture network are described as

$$v_{\mathrm{m}i} = -\frac{k_{\mathrm{m}ij}}{\phi_{\mathrm{m}} \mu_{\mathrm{m}}}\left(\frac{\partial p_{\mathrm{m}}}{\partial x_j} + \rho_{\mathrm{m}} g \frac{\partial z}{\partial x_j}\right) \tag{12a}$$

and

$$v_{\mathrm{f}i} = -\frac{k_{\mathrm{f}ij}}{\phi_{\mathrm{f}}\mu_{\mathrm{f}}}\left(\frac{\partial p_{\mathrm{f}}}{\partial x_j} + \rho_{\mathrm{f}} g \frac{\partial z}{\partial x_j}\right) \tag{12b}$$

$D_{\mathrm{m}ij}$ and $D_{\mathrm{f}ij}$ are the hydrodynamic dispersion tensors, which may be defined as

$$D_{\mathrm{m}ij} = (\alpha_{\mathrm{mL}} - \alpha_{\mathrm{mT}})\frac{v_{\mathrm{m}i}v_{\mathrm{m}j}}{|v_{\mathrm{m}}|} + \alpha_{\mathrm{mT}}|v_{\mathrm{m}}|\delta_{ij} + D_m^*, \quad i,j = 1,2 \tag{13a}$$

and

$$D_{\mathrm{f}ij} = (\alpha_{\mathrm{fL}} - \alpha_{\mathrm{fT}})\frac{v_{\mathrm{f}i}v_{\mathrm{f}j}}{|v_{\mathrm{f}}|} + \alpha_{\mathrm{fT}}|v_{\mathrm{f}}|\delta_{ij} + D_{\mathrm{f}}^*, \quad i,j = 1,2 \tag{13b}$$

where α_{mL} and α_{mT} are the longitudinal and transverse dispersivities, respectively, in the porous blocks, D_{f}^* is the coefficient of molecular diffusion and α_{fL} and α_{fT} are the longitudinal and transversal dispersivities, respectively, in the fracture network.

The initial and boudary conditions necessary for the contaminant transport equations (8) and (9) are

$$c_{\mathrm{m}} = c_{\mathrm{m}0} \quad \text{when } t = 0$$

$$c_{\mathrm{f}} = c_{\mathrm{f}0} \quad \text{when } t = 0$$

$$c_{\mathrm{m}} = \bar{c}_{\mathrm{m}} \quad \text{on } S_{\mathrm{mc}1}$$

$$\left(-\phi_{\mathrm{m}} D_{\mathrm{m}ij}\frac{\partial c_{\mathrm{m}}}{\partial x_i} + v_{\mathrm{m}i}\phi_{\mathrm{m}} c_{\mathrm{m}}\right)n_i = \bar{q}_{\mathrm{m}n}\bar{\bar{c}}_{\mathrm{m}} \quad \text{on } S_{\mathrm{mc}2}$$

$$c_{\mathrm{f}} = \bar{c}_{\mathrm{f}} \quad \text{on } S_{\mathrm{fc}1}$$

$$-\left(\phi_{\mathrm{f}} D_{\mathrm{f}ij}\frac{\partial c_{\mathrm{f}}}{\partial x_i} + v_{\mathrm{f}i}\phi_{\mathrm{f}} c_{\mathrm{f}}\right)n_i = \bar{q}_{\mathrm{f}n}\bar{\bar{c}}_{\mathrm{f}} \quad \text{on } S_{\mathrm{fc}2}$$

where $c_{\mathrm{m}0}$ and $c_{\mathrm{f}0}$ are the initial concentration in the porous blocks and the fracture network; $\bar{c}_{\mathrm{m}}$ and $\bar{c}_{\mathrm{f}}$ represent the prescribed concentration on boundaries $S_{\mathrm{mc}1}$ and $S_{\mathrm{fc}1}$; n_i is the unit vector normal to the boundaries, and $\bar{\bar{c}}_{\mathrm{m}}$ and $\bar{\bar{c}}_{\mathrm{f}}$ represent the prescribed concentration associated with prescribed fluid fluxes.

The density is assumed to be a function of concentration,

$$\rho_{\mathrm{m}} = \rho_{\mathrm{m}0} + \frac{\partial \rho_{\mathrm{m}}}{\partial c_{\mathrm{m}}}(c_{\mathrm{m}} - c_{\mathrm{m}0}) \tag{14}$$

$$\rho_{\mathrm{f}} = \rho_{\mathrm{f}0} + \frac{\partial \rho_{\mathrm{f}}}{\partial c_{\mathrm{f}}}(c_{\mathrm{f}} - c_{\mathrm{f}0}) \tag{15}$$

where $\rho_{\mathrm{m}0}$ and $\rho_{\mathrm{f}0}$ are fluid densities when $c_{\mathrm{m}} = c_{\mathrm{m}0}$ and $c_{\mathrm{f}} = c_{\mathrm{f}0}$, respectively.

3. FINITE ELEMENT APPROXIMATION

The system of differential equations (1), (2), (8) and (9) has been first approximated using standard Galerkin approach along with the upwind scheme, and then integrated numerically with respect to time.

In the upwind finite element scheme,[18, 19] the dispersion and advection terms of transient contaminant transport equations are weighted using asymmetric weighting functions to avoid oscillatory nature of the solution, whereas the time derivative term and the transmissive term are weighted using conventional shape functions.

Application of the standard Galerkin approach to equations (1) and (2) leads to

$$\rho_{\mathrm{m}} s_{\mathrm{m}}[M]\left[\frac{\partial p_{\mathrm{m}}}{\partial t}\right] + \phi_{\mathrm{m}} \frac{\partial \rho_{\mathrm{m}}}{\partial c_{\mathrm{m}}}[M]\left[\frac{\partial c_{\mathrm{m}}}{\partial t}\right] + ([T_1] + \rho_{\mathrm{m}}\eta[M])[p_{\mathrm{m}}] - \rho_{\mathrm{m}}\eta[M][p_{\mathrm{f}}] = [T_3] \tag{16}$$

$$\rho_{\mathrm{f}} s_{\mathrm{f}}[M]\left[\frac{\partial p_{\mathrm{f}}}{\partial t}\right] + \phi_{\mathrm{f}} \frac{\partial \rho_{\mathrm{f}}}{\partial c_{\mathrm{f}}}[M]\left[\frac{\partial c_{\mathrm{f}}}{\partial t}\right] + ([T_2] + \rho_{\mathrm{f}}\eta[M])[p_{\mathrm{f}}] - \rho_{\mathrm{f}}\eta[M][p_{\mathrm{m}}] = [T_4] \tag{17}$$

where

$$[M] = \int_A [N]^{\mathrm{T}}[N]\,\mathrm{d}A$$

$$[T_1] = \int_A \rho_{\mathrm{m}} \frac{k_{\mathrm{m}ij}}{\mu_{\mathrm{m}}} \frac{\partial [N]^{\mathrm{T}}}{\partial x_i} \frac{\partial [N]}{\partial x_j}\,\mathrm{d}A$$

$$[T_2] = \int_A \rho_{\mathrm{f}} \frac{k_{\mathrm{f}ij}}{\mu_{\mathrm{f}}} \frac{\partial [N]^{\mathrm{T}}}{\partial x_i} \frac{\partial [N]}{\partial x_j}\,\mathrm{d}A$$

$$[T_3] = -\int_A \rho_{\mathrm{m}}^2 g \frac{k_{\mathrm{m}ij}}{\mu_{\mathrm{m}}} \frac{\partial [N]^{\mathrm{T}}}{\partial x_i} \frac{\partial z}{\partial x_j}\,\mathrm{d}A - \int_A [N]^{\mathrm{T}} \rho_{\mathrm{m}} \eta(\rho_{\mathrm{m}} - \rho_{\mathrm{f}}) gz\,\mathrm{d}A - \int_S [N]^{\mathrm{T}} \rho_{\mathrm{m}} \bar{q}_{\mathrm{m}n}\,\mathrm{d}S$$

$$[T_4] = -\int_A \rho_{\mathrm{f}}^2 g \frac{k_{\mathrm{f}ij}}{\mu_{\mathrm{f}}} \frac{\partial [N]^{\mathrm{T}}}{\partial x_i} \frac{\partial z}{\partial x_j}\,\mathrm{d}A + \int_A [N]^{\mathrm{T}} \rho_{\mathrm{f}} \eta(\rho_{\mathrm{m}} - \rho_{\mathrm{f}}) gz\,\mathrm{d}A - \int_S [N]^{\mathrm{T}} \rho_{\mathrm{f}} \bar{q}_{\mathrm{f}n}\,\mathrm{d}S \quad i, j = 1,2$$

$[N]$ = shape function matrix.

In equations (16) and (17), densities ρ_{m} and ρ_{f} are employed using average densities $\rho_{\mathrm{m\,avg}}$ and $\rho_{\mathrm{f\,avg}}$ at all points in the element.[1]

Applications of the upwind finite element scheme to equations (8) and (9) leads to

$$R_{\mathrm{m}}\phi_{\mathrm{m}}[M]\left[\frac{\partial c_{\mathrm{m}}}{\partial t}\right] + ([T_5] + (\lambda R_{\mathrm{m}}\phi_{\mathrm{m}} + \beta)[M] + [T_7])[c_{\mathrm{m}}] - (\beta[M] - [T_8])[c_{\mathrm{f}}] = [Q_1] \tag{18}$$

$$R_{\mathrm{f}}\phi_{\mathrm{f}}[M]\left[\frac{\partial c_{\mathrm{f}}}{\partial t}\right] + ([T_6] + (\lambda R_{\mathrm{f}}\phi_{\mathrm{f}} + \beta)[M] - [T_8])[c_{\mathrm{f}}] - (\beta[M] - [T_7])[c_{\mathrm{m}}] = [Q_2] \tag{19}$$

where

$$[T_5] = \int_A \phi_m \left(D_{mij} \frac{\partial [W]^T}{\partial x_i} \frac{\partial [N]}{\partial x_j} + v_{mi} [W]^T \frac{\partial [N]}{\partial x_i} \right) dA$$

$$[T_6] = \int_A \phi_f \left(D_{fij} \frac{\partial [W]^T}{\partial x_i} \frac{\partial [N]}{\partial x_j} + v_{fi} [W]^T \frac{\partial [N]}{\partial x_i} \right) dA$$

$$[T_7] = \int_A (1 - d_1) \frac{\Gamma_1}{\rho_w} [N]^T [N] \, dA$$

$$[T_8] = \int_A d_1 \frac{\Gamma_1}{\rho_w} [N]^T [N] \, dA$$

$$[Q_1] = \int_S \phi_m [W]^T D_{mij} \frac{\partial c_m}{\partial x_j} n_i \, dS$$

$$[Q_2] = \int_S \phi_f [W]^T D_{fij} \frac{\partial c_f}{\partial x_j} n_i \, dS \quad i, j = 1, 2$$

$[W]$ = an asymmetric weighting function matrix.

For a four-node isoparametric finite element, the conventional shape functions are well known and need not to be repeated here. The expressions of asymmetric weighting functions of the element can be written as follows

$$W_1 = \tfrac{1}{16} [(1 + \bar{\xi})(-3\alpha_2 \bar{\xi} + 3\alpha_2 + 2)][(1 + \bar{\eta})(-3\beta_1 \bar{\eta} + 3\beta_1 + 2)]$$

$$W_2 = \tfrac{1}{16} [(1 + \bar{\xi})(3\alpha_2 \bar{\xi} - 3\alpha_2 - 2) + 4][(1 + \bar{\eta})(-3\beta_2 \bar{\eta} + 3\beta_2 + 2)]$$

$$W_3 = \tfrac{1}{16} [(1 + \bar{\xi})(3\alpha_1 \bar{\xi} - 3\alpha_1 - 2) + 4][(1 + \bar{\eta})(3\beta_2 \bar{\eta} - 3\beta_2 - 2) + 4]$$

$$W_4 = \tfrac{1}{16} [(1 + \bar{\xi})(-3\alpha_1 \bar{\xi} + 3\alpha_1 + 2)][(1 + \bar{\eta})(3\beta_1 \bar{\eta} - 3\beta_1 - 2) + 4]$$

where $\bar{\xi}$ and $\bar{\eta}$ are local co-ordinates; α_1, β_1, α_2 and β_2 are upwind parameters related to the sides of the element. The vaues of these parameters are dependent on the Courant number of element side and their optimal values have given by Huyakorn and Nikuha.[19]

The solution of equations (16)–(19) are obtained by a time-integration scheme. The integration over time internal Δt is performed in such a way that,

$$\int_t^{t+\Delta t} c \, dt = (\omega c^{t+\Delta t} + (1 - \omega) c^t) \Delta t \tag{20}$$

$$\Delta c = c^{t+\Delta t} - c^t$$

From equation (20), we can obtain a number of difference schemes by choosing the value of ω. A value of $\omega = 0$ indicates forward difference scheme, $\omega = 1$ indicates backward-difference scheme, and $\omega = 0{\cdot}5$ corresponds to Crank–Nicolson scheme. Using (20), equations (16)–(19)

yield the following set of algebraic equations:

$$\left[\frac{[F_{2w}]}{\Delta t}+\omega[F_{1w}]\right][p]^{t+\Delta t}+\frac{[F_{3w}]}{\Delta t}[c]^{t+\Delta t}=\left[\frac{[F_{2w}]}{\Delta t}-(1-\omega)[F_{1w}]\right][p]^{t}$$
$$+\frac{[F_{3w}]}{\Delta t}[c]^{t}+[\omega[F_{4w}]^{t+\Delta t}+(1-\omega)[F_{4w}]^{t}] \tag{21}$$

$$\left[\frac{[F_{2c}]}{\Delta t}+\omega[F_{1c}]\right][c]^{t+\Delta t}=\left[\frac{[F_{2c}]}{\Delta t}-(1-\omega)[F_{1c}]\right][c]^{t}$$
$$+[\omega[F_{3c}]^{t+\Delta t}+(1-\omega)[F_{3c}]^{t}] \tag{22}$$

where

$$[F_{1w}]=\begin{bmatrix}[T_1]+\rho_m\eta[M] & -\rho_m\eta[M]\\ -\rho_f\eta[M] & [T_2]+\rho_f\eta[M]\end{bmatrix},\qquad [F_{2w}]=\begin{bmatrix}\rho_m s_m[M] & [0]\\ [0] & \rho_f s_f[M]\end{bmatrix}$$

$$[F_{3w}]=\begin{bmatrix}\phi_m\dfrac{\partial\rho_m}{\partial c_m}[M] & [0]\\ [0] & \phi_f\dfrac{\partial\rho_f}{\partial c_f}[M]\end{bmatrix},\qquad [F_{4w}]=\begin{bmatrix}[T_3]\\ [T_4]\end{bmatrix}$$

$$[F_{1c}]=\begin{bmatrix}[T_5]+(\lambda R_m\phi_m+\beta)[M]+[T_7] & -(\beta[M]+[T_8])\\ -(\beta[M]+[T_7]) & [T_6]+(\lambda R_f\phi_f+\beta)[M]+[T_8]\end{bmatrix},$$

$$[F_{2c}]=\begin{bmatrix}R_m\phi_m[M] & [0]\\ [0] & R_f\phi_f[M]\end{bmatrix},\qquad [F_{3c}]=\begin{bmatrix}[Q_1]\\ [Q_2]\end{bmatrix}$$

$$[c]=\begin{bmatrix}[c_m]\\ [c_f]\end{bmatrix},\qquad [p]=\begin{bmatrix}[p_m]\\ [p_f]\end{bmatrix}$$

where ω is a weighting factor, $0\leqslant\omega\leqslant 1$, Δt is the time increment, $\omega=0{\cdot}5$ is used in this study.

Numerical accuracy and stability are maintained by using the Peclet and Courant criteria which are defined as,[1, 20,21]

$$Pe=v\frac{\Delta l}{D}\leqslant 2 \tag{23}$$

$$Cr=v\frac{\Delta t}{\Delta l}\leqslant 1 \tag{24}$$

where Δl is the local distance between the sides of an element along the local flow direction, v is the local velocity, and D is the hydrodynamic dispersion coefficient.

4. ITERATION TECHNIQUES FOR NON-LINEAR EQUATIONS

The density-dependent non-linearity in equations (21) and (22) is handled using the Picard method.[22] Starting from an initial estimate of concentration values in the fracture network and the porous blocks, the pressure and velocity values are obtained using equations (21), (12a) and (12b), respectively. The velocity values obtained are then used to solve for concentration values from equation (22). The same time step is used for all transient calculations. Iterations are performed until successive changes in nodal values of pressure p and concentration c in the fracture network and the porous blocks are within the prescribed tolerance limits.

$$\text{Max}|p_i^j - p_i^{j-1}| \leqslant \varepsilon \quad \text{and} \quad \text{Max}|c_i^j - c_i^{j-1}| \leqslant \varepsilon \quad \text{for } i = \text{f, m} \tag{25}$$

5. VALIDATION OF THE FORMULATION AND APPLICATIONS

To validate the finite element formulation and demonstrate the application of the numerical algorithm presented, a number of problems has been solved.

5.1. *Henry's problem*

The steady-state seawater intrusion in a homogeneous, isotropic, confined, rectangular aquifer was formulated using the approximate analytical solution to Henry.[23] Generally, density-dependent transport models are verified by comparison with the Henry problem. Huyakorn and Taylor[24] used three different finite element models to obtain the Henry solution. Voss and Souza[1] developed the SUTRA model to simulate the Henry's problem. To date, no model has successfully matched the Henry solution even for simulation times which approach steady state. However, a number of numerical models based on different methods give results nearly identical to one another for the Henry's problem. This evidence indicates that some inaccuracy in Henry's results may be due to missing higher-order terms which were originally dropped by Henry for the sake of reducing computational time.[1] In order to compare the proposed variable density models with the Henry's problem which is based on single porosity. Equations (1), (2), (8) and (9) are simplified to a signle porosity model by assuming flow and mass transfer term $\Gamma_1 = \Gamma_2 = 0$. Figure 1 shows the finite element mesh and the specified boundary conditions. The four-node quadrilateral finite element grid of 200 elements (231 nodes) is used here and the element size is $0{\cdot}1\text{ m} \times 0{\cdot}1\text{ m}$. The parameters chosen to match Henry's problem[1, 24] are as follows;

salt density $\rho_s = 1025\text{ kg/m}^3$

intrinsic permeability $k_{m11} = k_{m22} = 1{\cdot}02 \times 10^{-9}\text{ m}^{-2}$

$g = 9{\cdot}8\text{ m/s}^2$

dispersion coefficient $D_{m11} = D_{m22} = 6{\cdot}6 \times 10^{-6}\text{ m}^2/\text{s}$

$\alpha_{mL} = \alpha_{m1} = 0{\cdot}0$; $\beta = \eta = 0{\cdot}0$

$q = 6{\cdot}6 \times 10^{-5}\text{ m}^{-2}/\text{s}$

The concentration at the bottom of the aquifer after 100 min is compared with that obtined by Huyakorn and Taylor[24] and Voss and Souza[1] (Figure 2). It can be seen that the results compare very well.

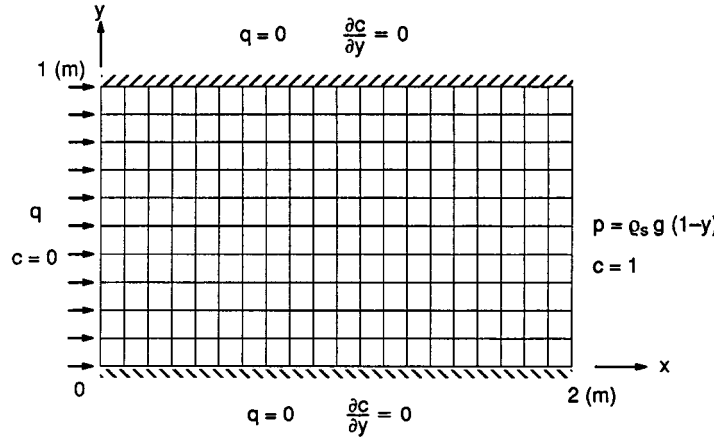

Figure 1. Finite element mesh and boundary conditions for Henry's Problem.

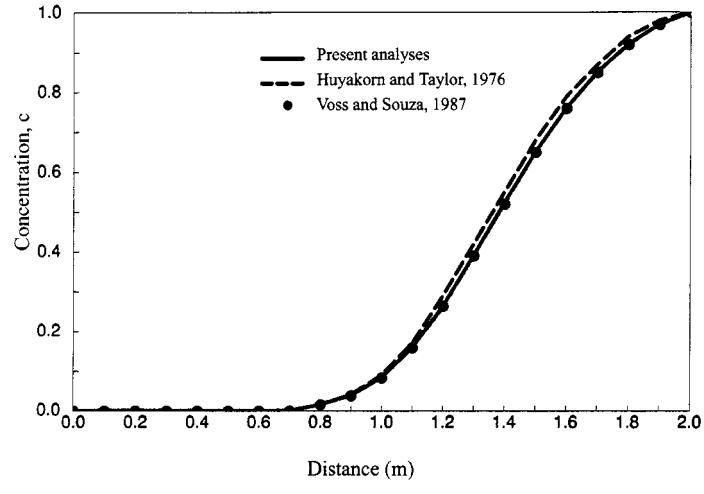

Figure 2. Comparison of concentration along the bottom of aquifer.

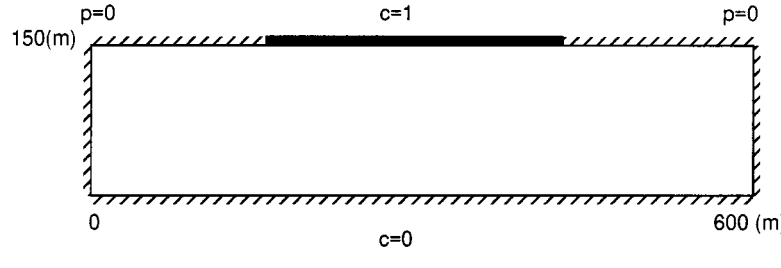

Figure 3. Boundary conditions for Elder problem.

5.2. *Elder problem*

The numerical results for Elder[25] for the problem of natural convection provide a useful basis for testing transport simulators in the case of flow driven purely by fluid density differences. The problem consists of a closed rectangular box with a source of solute at the top which is specified as a concentration boundary condition (Figure 3). The concentration along the entire bottom is specified at zero. The solute enters the initially pure water by diffusion, increase its density, and thereby begins a circulation process. Elder problem has been simulated by Voss and Souza[1] using the SUTRA model. To simulate their solution using the present model, the following data is used to match Elder's dimensionless results.[1]

porosity $\phi_m = 0{\cdot}1$

$g = 9{\cdot}8\ \mathrm{m/s^2}$

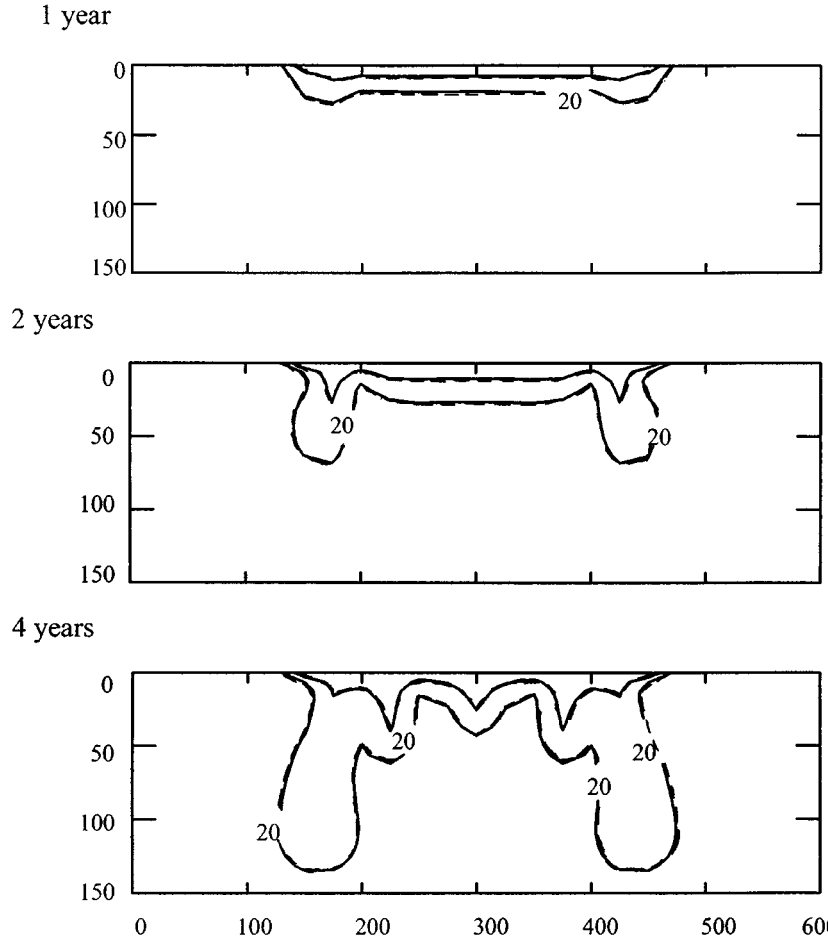

Figure 4. Comparison of dimensionless results with Voss and Souza[1], showing 20 and 60 per cent of maximum concentration contours

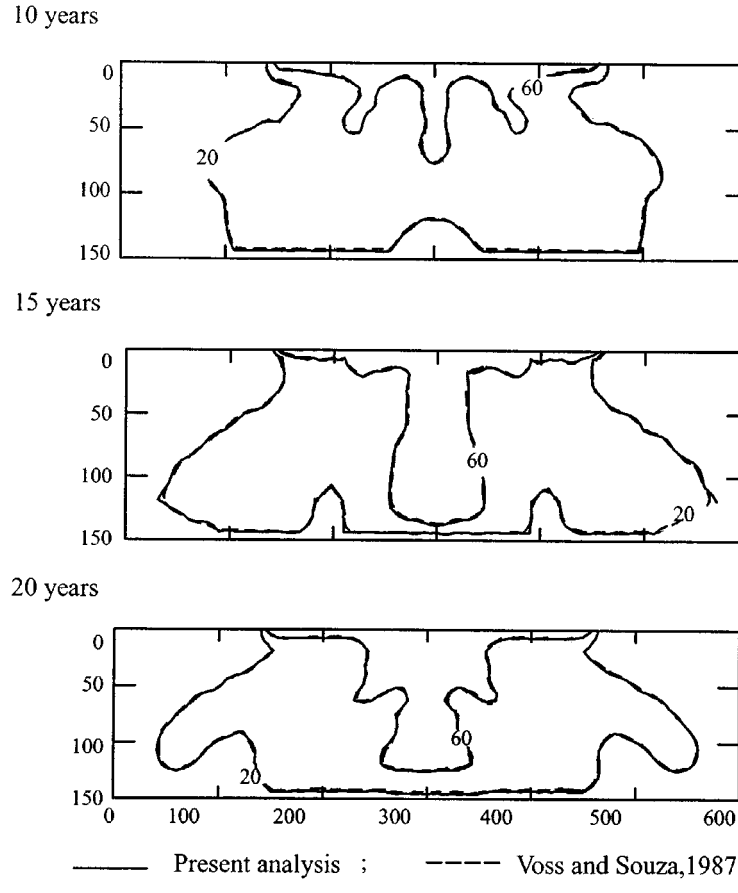

Figure 4. Continued

intrinsic permeability $k_{m11} = k_{m22} = 4{\cdot}845 \times 10^{-13}\ \mathrm{m}^2$

viscosity $\mu = 1{\cdot}0 \times 10^{-3}$ kg/m.s

diffusion $D_m^* = 3{\cdot}565 \times 10^{-6}\ \mathrm{m}^{-2}/\mathrm{s}$

$\rho = 1000\ \mathrm{kg/m}^3 + 200\ \mathrm{c}$
$\alpha_{mL} = \alpha_{m1} = 0{\cdot}0;\ \beta = \eta = 0{\cdot}0$

$c_{initial} = 0{\cdot}0$

A four-node quadirlateral finite element grid of 44 elements horizontally and 25 elements vertically (1100 elements and 1170 nodes) is used. The simulation is carried out with time step of one month, and iterations for each time step are desired to complete when the maximum absolute change for all nodes from the previous iteration falls below 500 pa for pressure and 0·01 for concentration.

Figure 4 compares the results of present simulation to those of Voss and Souza.[1] The results compare very well, spatially and through time, showing that both numerical solutions give similar representation of the complex density-driven flow and solute transport behaviour.

5.3. *Contamination migration in fractured porous media*

To demonstrate the application of the proposed formulation, the problem of a shallow surface impoundment located over a fractured aquifer, approximately 900 m long and 90 m deep, is considered. The surface impoundment is 100 m wide and is located 200 m from the left boundary of the aquifer. A static hydraulic head difference of 2·0 m is assumed to exist between left and right boundaries of the aquifer. No-flux boundaries are assumed at the top and the base.

The geometry and the boundary conditions of the problem are shown in Figure 5. The problem is similar to that investigated by Koch and Zhang,[4] except that the aquifer is assumed to be fracture. A finite element grid of 1232 elements (1326 nodes) is used in the analysis.

The parameters used are: the fracture network permeability $k^0_{f11} = k^0_{f22} = 10^{-12}\,\mathrm{m}^2$; the porous blocks permeability $k^0_{m11} = k^0_{m22} = 10^{-14}\,\mathrm{m}^2$; viscosity $\mu = 1{\cdot}15 \times 10^{-18}\,\mathrm{N\,day/m}^2$; porosity in the fracture network $\phi_f = 0{\cdot}001$; porosity in the porous blocks $\phi_m = 0{\cdot}05$; leakage parameter $\eta = 2{\cdot}4 \times 10^{-3}\,\mathrm{m}^2/\mathrm{N\,day}$; mass transfer parameter $\beta = 1{\cdot}2 \times 10^{-4}\,\mathrm{day}^{-1}$; dispersivities in the fracture network and the porous block $\alpha_{fL} = \alpha_{mT} = 0{\cdot}5$ m. The parameters adopted are typical of fractured siltstone. Two types of surface impoundment are considered: (1) infinite source and (2) finite source. In both cases, the contaminant is assumed to be conservative with $\lambda = 0$ and $R = 1$.

5.3.1. Infinite source. In this case, the surface impoundment is assumed to be of inifinite supply with a concentration of unity at the surface of the aquifer. The density of the contaminant is assumed to be $\rho = 1200\,\mathrm{kg/m}^3$, typical of a highly concentrated brine.

The results of the analysis in terms of contaminant concentration in the fracture network and the porous blocks are shown in Figures 6–8. Two different cases are analysed: (1) infiltration with the density effect include and (2) infiltration without the density effects. Figures 6(a)–8(a) show the concentration in the fracture network and the porous blocks at $t = 1 \times 10^3$, 1×10^4, 5×10^4 h (42, 417, 2083 days) for the case where the density effect is not included, whereas Figures 6(b)–8(b) show the results for the case where the density effect is included. By comparing the results between the two cases, it can be seen that with increased time, the spread of the contamination in the fracture network and the porous blocks is significantly larger in the case where the density effect is included.

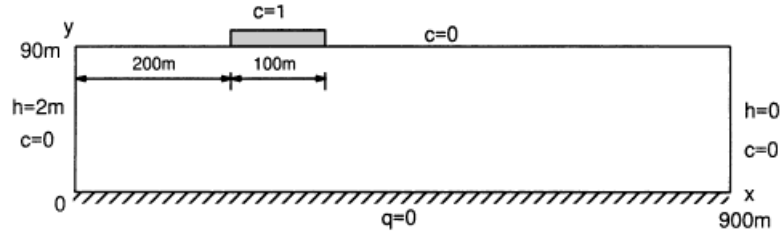

Figure 5. Geometry and boundary conditions for fractured porous aquifer

From Figures 6–8 it can also be seen that initially, the contaminant transport occurs mainly in the fractures. With increased time, the fracture network starts leaking into the porous blocks and the contaminant concentration in the porous blocks increases. Eventually, during the later periods, concentrations in the fracture network and the porous block reach similar values, but not corresponding to the steady-state equivalent homogeneous behaviour of the total system, because of the velocity-dependent dispersion.

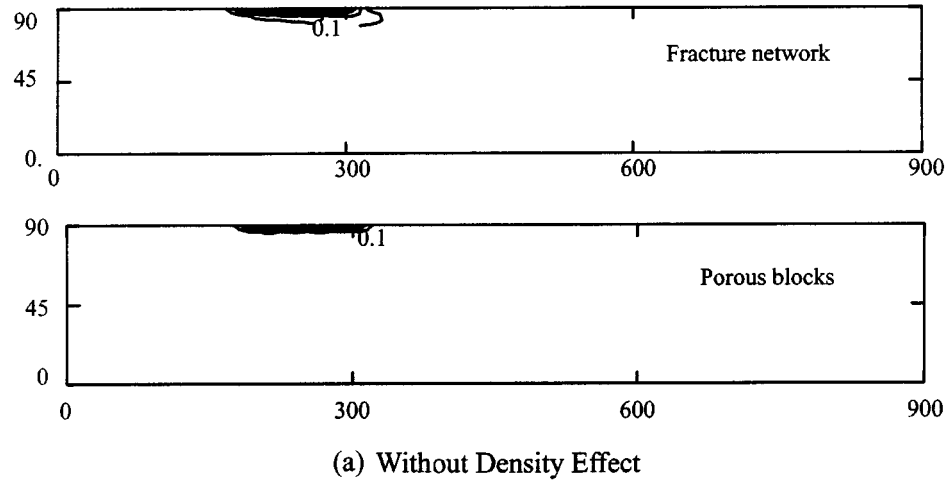

(a) Without Density Effect

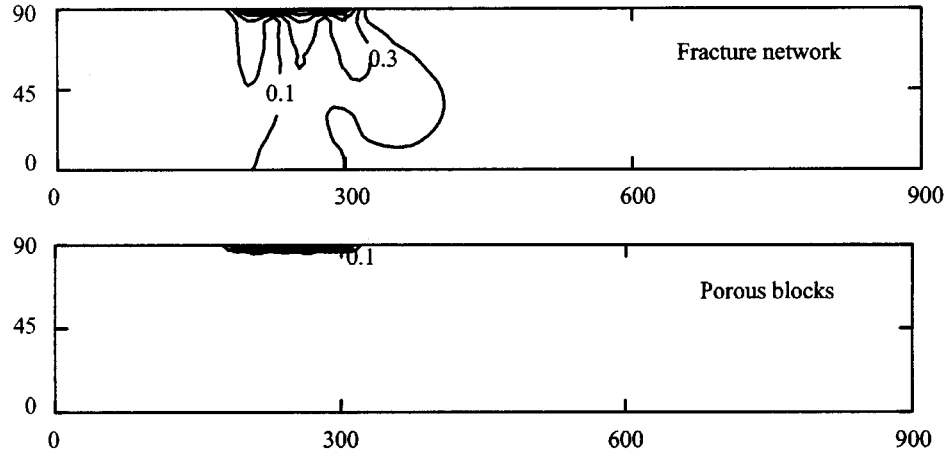

(b) With Density Effect

Figure 6. Concentration of contaminant in fracture network and porous blocks after 42 days, (a) without density effect (neutral density) and (b) with density effect

Figure 9 shows the concentration at the observation point of $x = 300$ m and $y = 30$ m versus time. It is shown that, as time increases, the concentrtion in the fracture network approaches a similar value as in the porous blocks, but different from that obtained using an equivalent single porosity model. Figure 10 shows the results in the case where the dispersion is assumed to be zero; i.e. $D_m^* = D_f^* = 0{\cdot}01$ m^2/h. Other parameters being the same as before, a finite element grid of 1242 elements (1390 nodes) is used to satisfy the Peclet and Courant criteria. As can be noted, in this case, during the late time period, the concentration in the fractured porous medium approaches

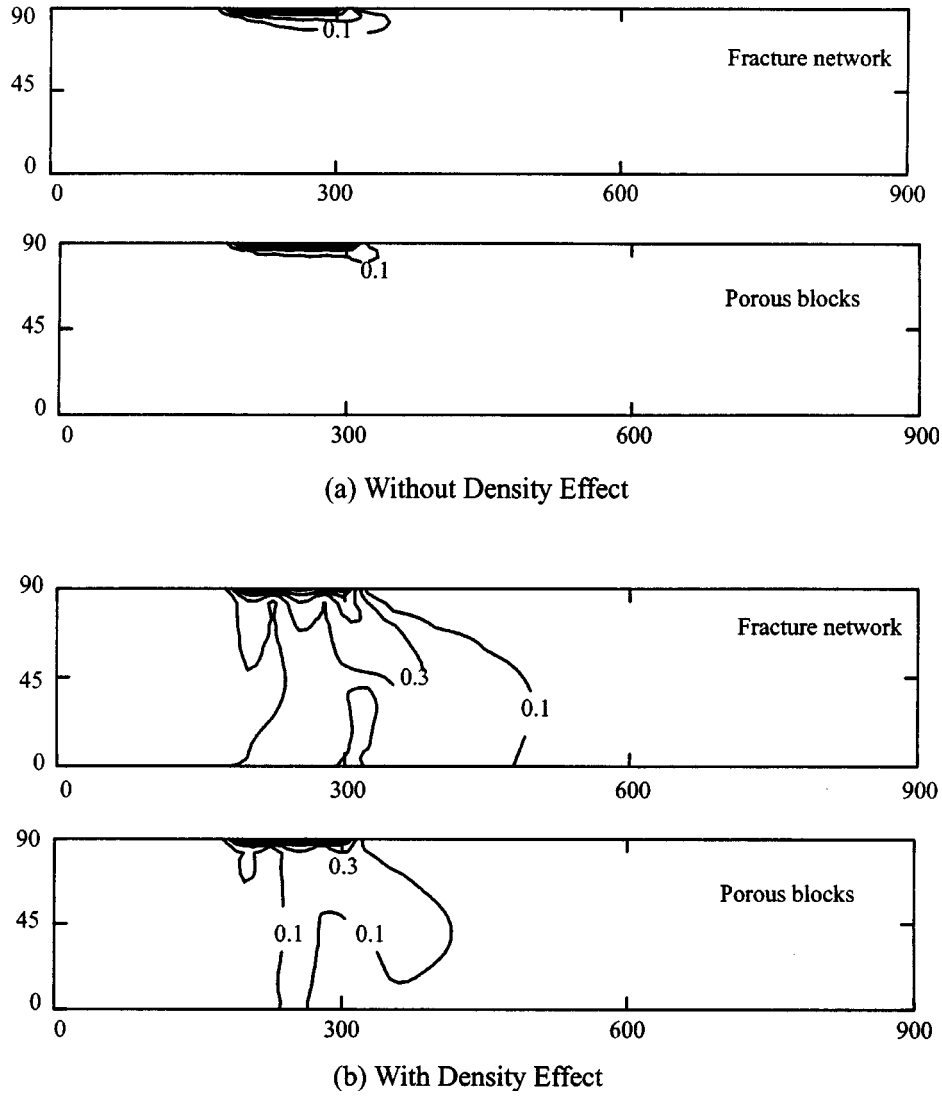

Figure 7. Concentration of contaminant in fracture network and porous blocks after 417 days, (a) without density effect (neutral density) and (b) with density effect

the one observed in the homogeneous medium. Therefore, in order to determine the response of closely fractured regions over a long period, the conventional homogeneous model can only be used in the diffusion-type problems.

5.3.2. Finite source. In this case, the surface impoundment is assumed to be of limited supply. The volume of contaminant is finite, and the surface infiltration occurs only over a limited period

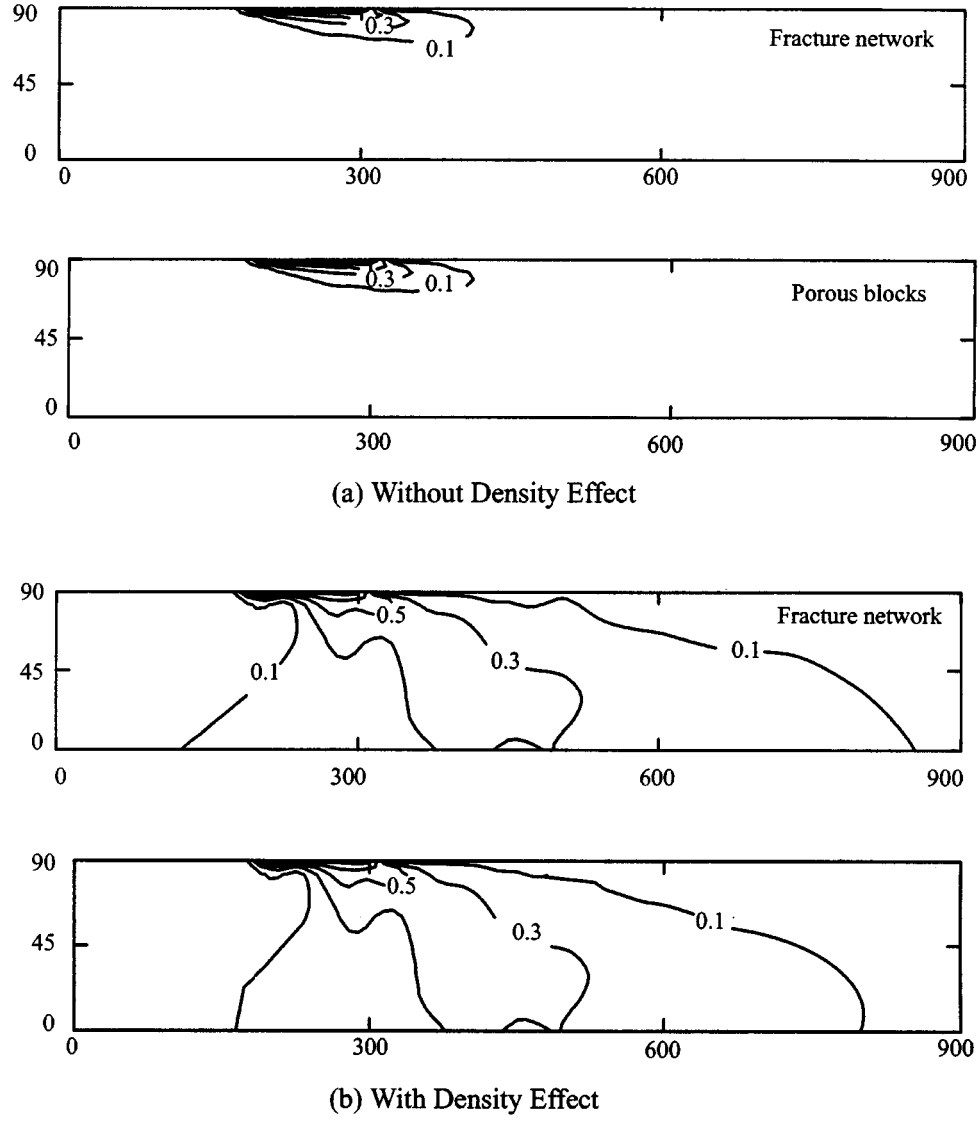

Figure 8. Concentration of contaminant in fracture network and porous blocks after 2083 days, (a) without density effect (neutral density) and (b) with density effect

of time (i.e 5×10^3 h or 208 days, in this case). The contaminant concentration at the impoundment is assumed to be unity prior to 5×10^3 h, and zero thereafter. Other parameters are assumed to be the same as before. The results of the analysis in terms of contaminant concentration at observation points ($x = 310$, $y = 80$ m) and ($x = 275$, $y = 85$ m) versus time are shown in Figure 11. As can be seen, similar to the previous case, during the early stages the concentration of contaminant is primarily dominated by the fractures. As time increases, the fracture network starts leaking into the porous blocks and the contaminant concentration in the porous blocks increases gradually. This trend continues until the source of contamination is depleted at the

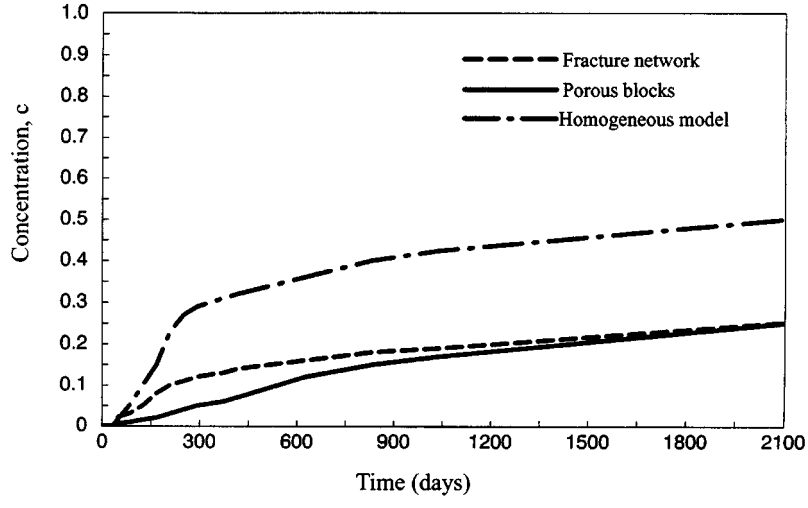

Figure 9. Concentration of contaminant at point ($x = 300$ m, $y = 30$ m) versus time (including diffusion and dispersion)

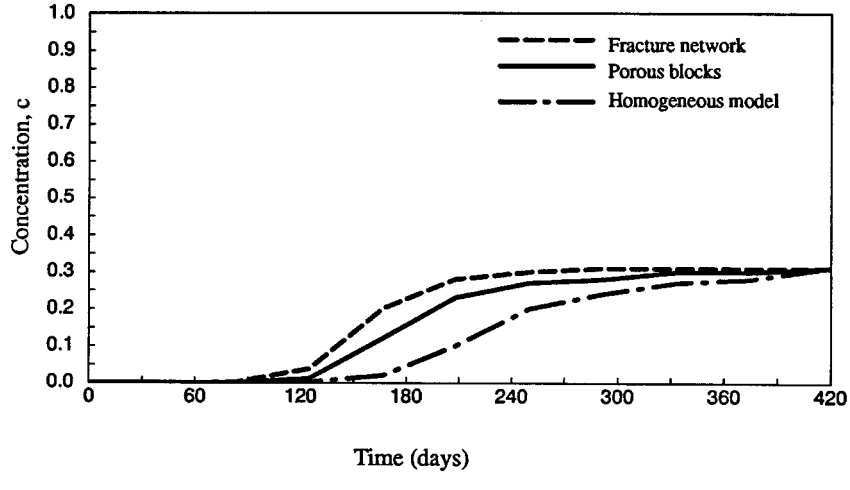

Figure 10. Concentration of contaminant at point ($x = 300$ m, $y = 30$ m) versus time (diffusion only)

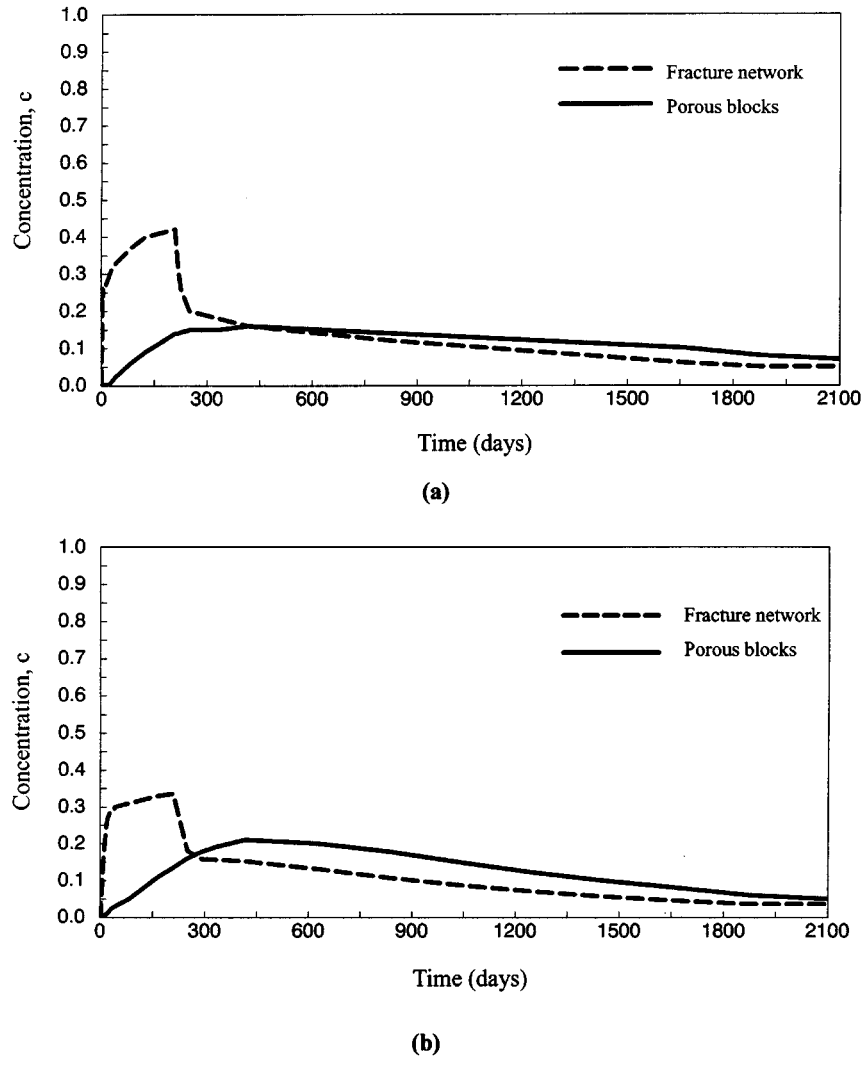

Figure 11. Concentration of contaminant versus time in fracture network and porous blocks at points (a) $x = 310$ m, $y = 80$ m and (b) $x = 275$ m, $y = 85$ m

surface. At this point, the concentration drops very rapidly in the fracture network, and it reaches a peak value in the porous blocks. Beyond this point, and at the subsequent times, concentrations in both the fracture network and the porous blocks decrease gradually until they reach negligible values at very large times. From Figure 11, it is also interesting to note that, during the early stages, the transfer of contaminant is from the fracture network to the porous blocks, whereas it is from the porous block to fracture network during the later time periods.

5.3.3. Effect of fracture spacing. Fracture spacing can affect the response of a fractured medium through changing the average permeability of the fracture network, k_f, the leakage

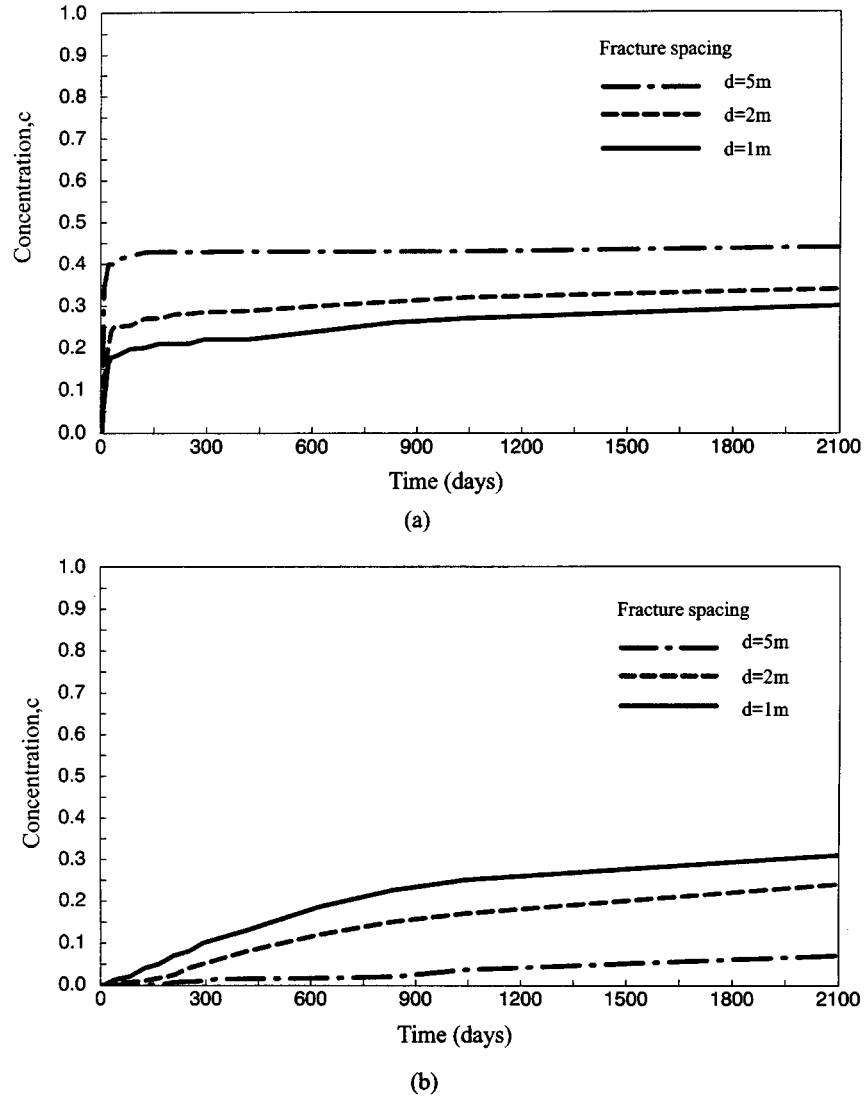

Figure 12. Concentration of contaminant versus time in (a) fracutre network an (b) porous blocks at point ($x = 350$ m, $y = 30$ m), using different values of fracture spacing

parameter, η, and the concentration transfer term, β. The values of these parameters decrease as the average fissure spacing increaes.

In this section, to investigate the effects of fracture spacing on contaminant transport, sensitivity analyses are performed using the problem described in Section 5.3.1 and three different fracture spacings of 1, 2 and 5 m. In all cases, the fluid density is $\rho = 1200$ kg/m^3 when $c = c_0$. The material properties adopted are as given in Table I.

Table I. Material properties employed in simulating contaminant migration in fractured porous media using different fracture spacing

	Fracture spacing		
	1 m	2 m	5 m
Viscosity, μ (N day/m^2)	$1{\cdot}15\times10^{-8}$	$1{\cdot}15\times10^{-8}$	$1{\cdot}15\times10^{-8}$
Permeability in porous blocks k_m (m^2)	10^{-14}	10^{-14}	10^{-14}
Permeability in fracture network k_f (m^2)	10^{-12}	5×10^{-13}	2×10^{-13}
Porosity in porous blocks ϕ_m	0·05	0·05	0·05
Porosity in fracture network ϕ_f	0.001	0·005	0·0002
Leakage parameter η (m^2/N day)	$2{\cdot}4\times10^{-3}$	6×10^{-4}	$9{\cdot}6\times10^{-5}$
Concentration transfer term β (day^{-1})	$1{\cdot}2\times10^{-4}$	3×10^{5}	$4{\cdot}8\times10^{-6}$
Longitudinal dispersivities in porous blocks a_{mL} (m)	5	5	5
Transverse dispersivities in porous blocks a_{mT} (m)	0·5	0·5	0·5
Longitudinal dispersivities in fracture network a_{fL} (m)	5	5	5
Transverse dispersivities in fracture network a_{fT} (m)	0·5	0·5	0·5

Figures 12 shows the effect of fracture spacing on concentration in fractured media and porous media at the observation point $x = 350$ m and $y = 30$ m. Comparing the results, it can be seen that as the fracture spacing increases, the concentration in fractured media increases and the concentration in porous decreases, as would be expected.

6. CONCLUSIONS

The formulation for variable density flow and contaminant transport in fractured porous media has been presented. The finite element method has been used as the numerical tool to implement the proposed formulation. The non-linearities arising from the density variation and the velocity-dependent dispersion terms have been handled by Picard method.

The formulation has been validated and applied to several problems involving the variable density flow and transport in fractured porous media. The results show that, initially the contaminant concentration is dominant in fractures. As the time increases the fracture network starts leaking into the porous blocks, and the contaminant in porous blocks increases. At this stage, the effect of density on concentration in the fracture network is more prominent than in the porous blocks. Eventually, at later periods, cocentrations in the fracture network and the porous blocks reach similar values. However, it should be noted that they are not the same as the equivalent homogeneous behaviour of the total system because of the velocity-dependent dispersion. In order to investigate the effect of other parameters such as spacing of fractures and porosity, parametric studies have been carried out and the results show the important of including the variable density in the formulation.

ACKNOWLEDGEMENTS

This study forms a part of the research program on contaminant transport, carried out in the School of Civil Engineering, University of New South Wales under the direction of the senior author.

REFERENCES

1. C. I. Voss and W. R. Souza, 'Variable density flow and solute transport simulation of regional aquifers containing a narrow freshwater–saltwater transition zone', *Water Resour. Res.*, **23,** 1851–1866 (1987).
2. A. M. Herbert, C. P. Jackson and D. A. Lever, 'Coupled groundwater flow and solute transport with fluid density strongly dependent upon concentration', *Water Resour. Res.*, **24,** 1781–1795 (1988).
3. H. W. Dorgarten and C. F. Tsang, 'Modelling density-driven movement of liquid waste in deep sloping aquifers', *Ground Water*, **29,** 655–662 (1991).
4. M. Koch and G. P. Zhang, 'Numerical simulation of the effects of variable density in a contaminant plume', *Ground Water*, **30,** 731–742 (1992).
5. B. E. Sleep and J. F. Sykes, 'Modelling the transport of volatile organics in variably saturated media', *Water Resour. Res.*, **15,** 81–92 (1989).
6. C. A. Mendoza and E. O. Frind, 'Advective-dispersive flow of dense organic vapors in the unsaturated zone, 1, Model development', *Water Resour. Res.*, **26,** 378–389 (1990).
7. R. A. Schincariol, F. W. Schwartz and C. A. Mendoza, 'On the generation of instabilities in variable density flow', *Water Resour. Res.*, **30**(4), 913–927 (1994).
8. H. Zhang and F. W. Schwartz, 'Multispecies contaminant plumes in variable density flow systems,' *Water Resour. Res.* **31**(4), 837–847 (1995).
9. C. M. Wicks and J. S. Herman, 'The effect of zones of high porosity and permeability on the configuration of the saline-freshwater mixing zone', *Ground Water*, **33**(5), 733–740 (1995).
10. G. I. Barenblatt, I. P. Zheltov and N. Kochina, 'Basic concepts in the theory of seepage of homogeneous liquids in fissured rocks', *J. Appl. Math. Mech.* **24,** 1286–1303 (1960).
11. J. E. Warren and P. J. Root, 'The behavior of naturally fractured reservoirs', *Soc. Pet. Engng. J.*, **3,** 245–255 (1963).
12. P. S. Huyakorn, B. H. Lester and C. R. Faust, 'Finite element techniques for modelling groundwater flow in fractured aquifers', *Water Resuor. Res.*, **19,** 1019–1035 (1983).
13. P. S. Huyakorn, B. H. Lester and J. W. Mercer, 'An efficient finite element techniques for modelling transport in fractured aquifers, 1. Single species transport', *Water Resour. Res.*, **19,** 841–854 (1983).
14. R. K. Rowe and J. R. Booker, 'Contaminant migration through fractured till into an underlaying aquifer', *Can. Geotech. J.*, **27,** 484–495 (1990).
15. S. G. Shikaze and E. A. Sudicky, 'Simulation of dense vapor migration in discretely fractured geologic media', *Water Resour. Res.*, **30,** 1993–2009 (1994).
16. S. Valliappan and N. Khalili-Naghadeh, 'Flow through fissured porous media with deformation matrix', *Int. J. Numer. Engng.* **29,** 1079–1094 (1990).
17. N. Khalili-Naghadeh and S. Valliappan, 'Flow through fissured porous media with deformable media: implicit formulation', *Water Resour. Res.* **27,** 1703–1709 (1991).
18. J. C. Heinrich, P. S. Huyakorn, O. C. Zienkiewicz and A. R. Michell, 'An upwind finite element scheme for two dimensional convection transport eqation', *Int. J. Numer. Meth. Engng.*, **11,** 131–143 (1977).
19. P. S. Huyakorn and K. Nikuha, 'Solution of transient transport equation using an upstream finite element scheme', *Appl. Math. Modelling*, **3,** 7–17 (1979).
20. A. D. Daus, E. O. Frind and E. A. Sudicky, 'Comparitive error analysis in finite-element formulations of the advection–dispersion equation', *Adv. Water Resour.*, **8,** 86–95 (1985).
21. P. S. Huyakorn and G. F. Pinder, *Computational Methods in Subsurface Flow*, Academic, San Diego, DA, 1983.
22. J. D. Istok, *Groundwater Modeling by the Finite Element Method*, American Geophysical Union, 1989.
23. H. R. Henry, 'Effects of dispersion on salt encroachment in coastal aquifers', *U.S. Geol. Surv. Water Supply Pap., 1613-C,* C71–C84 (1964).
24. P. S. Huyakorn and C. Taylor, 'Finite element models for coupled groundwater flow and convective dispersion', in *Finite Elements in Water Resources* Grat *et al.* (ed.,) Pentech, London, 1976, pp. 1.131–1.151.
25. J. W. Elder, 'Transient convection in a porous medium', *J. Fluid Mech.* **27,** 609–623 (1967).
26. J. Bear, *Dynamics of Fluids on Porous, Media*, Elsevier, New York, 1972.

